Transmission and reflection from a layered medium in water. Simulations and measurements

Espen Storheim[1,*], Kjetil Daae Lohne[1], and Torbjørn Hergum[2]

[1]Christian Michelsen Research AS, P.O. Box 6031, N-5892 Bergen, Norway
[2]Bergen Technology Center AS, Damsgårdveien 135, 5160 Laksevåg, Norway
[*]Contact author: Espen.Storheim@cmr.no

Abstract

A water immersed, plane layered medium, consisting of stainless steel and Plexiglas plates, has been experimentally investigated at normal incidence with through-transmission measurements. Experimental results of single and sandwiched plates have been compared to simulations with the global matrix method. A fair agreement between measurements and simulations is observed for transmission through single plates. Debonding has been visually observed in the sandwiched system and introduced in the simulation model in order to explain the discrepancies between original simulations and measurements. Simulations with debonding show a better correspondence with measured results.

1 Introduction

Condition monitoring of oil and gas wells has become increasingly more important over the years, due to the ecological and economical consequences associated with e.g. leakage. In addition, the amount of wells due for plug and abandonment is significant, and increasing. However condition monitoring of cement is challenging due to its porosity and the dependency of pressure, temperature, stress, etc. Hence, the actual conditions of the cement in the well is not known and makes it difficult to interpret the measurements. It is of interest to get a better understanding of the wave propagation in cement, and also for layered media. It is also of interest to use different simulation tools to design and optimize the measurement systems, and investigate the wave propagation in the different layers.

The oil well can be regarded as a layered medium which typically consists of a fluid, one or several steel casings, cement, and the formation. In such a system, it is of interest to determine the condition of the cement. This includes the bonding between the steel casing and the cement, the bonding between the cement and the formation, and detection of cracks or voids in the cement where oil or gas can flow through. However, preparing a uniform cement sample free of defects is difficult even under laboratory conditions, and the sample is also difficult to handle due to the recommendations for well cement samples in [1]. Thus, use of an alternative material which represents the cement can give useful information.

Wave propagation in layered media is widely discussed in the literature, such as [2–6]. The wave propagation through a periodically stratified medium is investigated by e.g. [7], where both the short and long wavelength is discussed. Lowe [8] has presented an overview of two different matrix techniques: the transfer matrix method (TMM) [9,10]; and the global matrix method (GMM) [11,12]. Brouard [13] has investigated the transmission and reflection for layered medium with simulations and measurements. Results are presented for the transmission coefficient as a function of incidence angle at certain frequencies, for one, two, and three finite layers immersed in water.

Simulation tools are important in the design and optimization of measurement systems. In recent years, finite element modeling (FEM) has become increasingly more popular with the continuous development of

multiphysics tools such as COMSOL [14]. Other methods are also available, such as the SimSonic toolbox [15], which uses the finite-difference time-domain method, and the k-wave toolbox [16], which uses a pseudospectral method. However, these methods are often time consuming and complicated. In certain cases, simplified plane-wave models can be useful as a first iteration.

The aim of the present work is to investigate the transmission properties for a layered medium which consists of two elastic plates immersed in water, and where the material parameters and physical dimensions of the plates are known. The layers are investigated separately with measurements and simulations to investigate the correspondence, and to identify the characteristic features. The results are in turn compared to measurements and simulations on the layered structure. The influence on the transmission coefficient due to debonding between the plates is also discussed.

2 Theory

2.1 An elastic plate immersed in a fluid

Consider a plane, longitudinal wave incident at an oblique angle θ_{L1} (from the normal vector of the surface) towards an elastic plate with thickness d, infinite in the horizontal plane (xy plane), and immersed in an inviscid fluid. The longitudinal and shear velocities for the different media are denoted by c_{Ln} and c_{Sn}, and the densities as ρ_n, where $n = 1, 2, 3$. It is in the following assumed that the fluids in the upper and lower halfspaces are equal, that the halfspaces are semi-infinite, and that the different materials are lossless. Absorption can however be taken into account through a complex wavenumber. Figure 1 shows an illustration of the transmission and reflection of an incident longitudinal wave towards the front surface of an elastic plate with thickness d, immersed in an inviscid fluid.

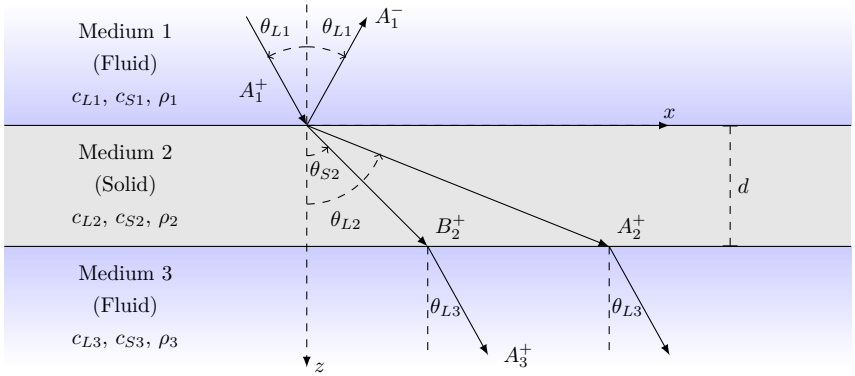

Figure 1: Illustration of the reflection and transmission of an incident longitudinal wave at an elastic plate with thickness d, placed between two semi-infinite fluid halfspaces. The internal reflections in medium 2 are not shown.

The boundary conditions on the fluid/elastic interface are continuity in the normal displacement u_z and the normal stress τ_{zz}, and zero shear stress, i.e. $\tau_{xz} = 0$. The amplitude of the longitudinal waves is denoted by $A_n^{\pm}$, and the shear wave amplitude by $B_n^{\pm}$, where n is the medium number, and $+$ or $-$ in the superscript indicates propagation in the positive (downward) or negative (upward) z direction, respectively. At the front surface of the plate, i.e. the interface between medium 1 and 2, a specular reflection of the longitudinal wave occurs, where the amplitude of the reflected wave is A_1^-. In the elastic material, a longitudinal and a shear wave are refracted, with respective amplitudes of A_2^+ and B_2^+. As these waves reach the second interface, longitudinal waves are refracted into the fluid medium. The refracted angles are governed by Snell's law as [8]

$$\frac{\sin(\theta_{L1})}{c_{L1}} = \frac{\sin(\theta_{L2})}{c_{L2}} = \frac{\sin(\theta_{S2})}{c_{S2}} = \frac{\sin(\theta_{L3})}{c_{L3}}. \tag{1}$$

The refracted waves can only exists below their critical angle, i.e. the incidence angle where the refracted angle

is 90°. When the longitudinal sound velocity in medium 1 and medium 3 are equal ($c_{L1} = c_{L3}$), the refracted angle in the lower halfspace is equal to the incident angle towards the plate, i.e.

$$\theta_{L3} = \arcsin\left(\frac{c_{L3}}{c_{L1}}\sin(\theta_{L1})\right) = \arcsin\left(\sin(\theta_{L1})\right) = \theta_{L1}, \tag{2}$$

cf. Eq. (1).

A propagating longitudinal wave has a longitudinal wavenumber $h = \omega/c_L$, where $\omega = 2\pi f$ is the angular frequency and f is the frequency, which consists of a horizontal and vertical component, denoted by h_x and h_z, respectively. This is expressed for the longitudinal wave in medium n as [17]

$$h_n^2 = \left(\frac{\omega}{c_{Ln}}\right)^2 = h_{n,x}^2 + h_{n,z}^2 = \left(h_n \sin(\theta_{Ln})\right)^2 + \left(h_n \cos(\theta_{Ln})\right)^2, \tag{3}$$

in terms of the angle from the vertical axis. Similarly, the shear wavenumber is defined as [17]

$$k_n^2 = \left(\frac{\omega}{c_{Sn}}\right)^2 = k_{n,x}^2 + k_{n,z}^2 = \left(k_n \sin(\theta_{S,n})\right)^2 + \left(k_n \cos(\theta_{S,n})\right)^2, \tag{4}$$

for propagating shear waves. The horizontal wavenumbers are equal for each material and will be denoted by η, i.e. $h_{n,x} = k_{n,x} \equiv \eta$, as shown by Snell's law for elastic materials. Only vertically polarized shear waves (SV) are included in the analysis, since the horizontal shear waves (SH) propagate in the xy plane, not in the z-direction. [8].

The pressure transmission and reflection coefficients are defined as the ratio between the transmitted and the incident pressure, and the ratio between the reflected pressure and the incident pressure, respectively. These coefficients for a fluid immersed plate are given as analytical expressions in [4] as

$$T_{13}^{LL} = \frac{2\alpha}{2\beta + i(\beta^2 - \alpha^2 - 1)}, \tag{5}$$

$$R_{11}^{LL} = \frac{2\alpha}{2\beta + i(\beta^2 - \alpha^2 - 1)}, \tag{6}$$

where $i = \sqrt{-1}$, and the coefficients α and β are given as

$$\alpha = \frac{\rho_2 c_{L2}\cos(\theta_{L1})\cos^2(2\theta_{S2})}{\rho_1 c_{L1}\cos(\theta_{L2})\sin(2h_2 L\cos(\theta_{L2}))} + \frac{\rho_2 c_{L2}\cos(\theta_{L1})\sin^2(2\theta_{S2})}{\rho_1 c_{L1}\cos(\theta_{L2})\sin(2h_2 L\cos(\theta_{L2}))}, \tag{7}$$

$$\beta = \frac{\rho_2 c_{L2}\cos(\theta_{L1})\cos^2(2\theta_{S2})}{\rho_1 c_{L1}\cos(\theta_{L2})\tan(2h_2 L\cos(\theta_{L2}))} + \frac{\rho_2 c_{L2}\cos(\theta_{L1})\sin^2(2\theta_{S2})}{\rho_1 c_{L1}\cos(\theta_{L2})\tan(2h_2 L\cos(\theta_{L2}))}, \tag{8}$$

with $L = d/2$ as the half plate thickness. The superscript used for the reflection and transmission coefficients denotes the type of incident and reflected/refracted wave, i.e. LL is longitudinal to longitudinal, and LS would be longitudinal to shear. The latter is however not used here as an inviscid fluid does not support shear waves. Similarly, the subscript indicates in which medium the wave propagates from and to, i.e. 13 is a wave incident in medium 1 and transmitted to medium 3.

For a plate with finite thickness d in vacuum, infinite in the xy plane, Rayleigh-Lamb modes exists in the plate. The higher order symmetric and antisymmetric modes, denoted by S_p and A_p ($p = 1, 2, \ldots$), have cutoff frequencies which is the lower limit where these modes exists. These cutoff frequencies are given as [18]

$$f_n^S = n\frac{c_S}{d}, \quad n = 1, 2, 3, \ldots, \qquad f_m^S = m\frac{c_L}{2d}, \quad m = 1, 3, 5, \ldots, \tag{9}$$

$$f_n^A = n\frac{c_L}{d}, \quad n = 1, 2, 3, \ldots, \qquad f_m^A = m\frac{c_S}{2d}, \quad m = 1, 3, 5, \ldots. \tag{10}$$

The zero order modes S_0 and A_0 exists for the entire frequency range. The longitudinal thickness resonance

frequencies for the elastic plate in vacuum are by manipulating Eqs. (9) and (10) expressed as

$$f_L^{(m)} = m\frac{c_L}{2d}, \qquad m = 1, 2, 3, \ldots, \tag{11}$$

where $c_L = c_{L2}$. It is in the present case assumed that Eq. (11) is valid for the steel plate immersed in water, due to the large contrast in characteristic impedance (ρc_L).

2.2 A layered medium between two semi-infinite halfspaces

For a layered medium, where several different plates with finite thickness are in contact, more complicated methods are required for calculation of the transmission and reflection coefficients. Figure 2 shows an illustration of the case considered in the present work, where an incident longitudinal wave in water is reflected and refracted at a layered medium with $N-2$ finite layers, placed between two semi-infinite fluid halfspaces.

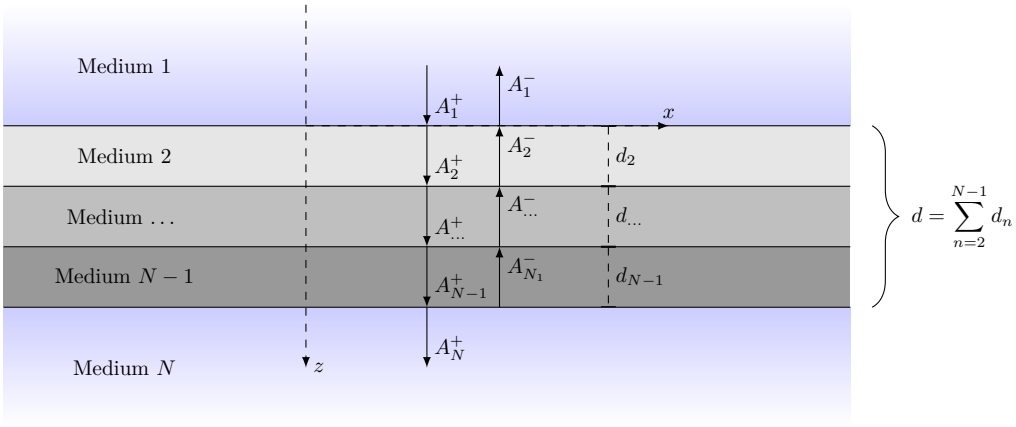

Figure 2: Illustration of the reflection and transmission of an incident longitudinal wave at normal incidence towards a layered medium with thickness d, placed between two semi-infinite fluid halfspaces. The total thickness of the sandwich is denoted d and is the sum of the thickness of each of the finite layers.

The method which has been implemented in the present work is the global matrix method. Even though the TMM is more computationally efficient compared to the GMM due to the size of the system matrix, numerical problems have been observed for large frequency times thickness (fd) products [8, 19]. The method is not restricted to fluid halfspaces as illustrated in Figure 2, and internal fluid layers are also supported. The outline of the method which is given in the present section is based on [8, 20].

The boundary conditions for a fluid/elastic interface is equal those given in Section 2.1, i.e. continuity in u_z and τ_{zz}, and $\tau_{zx} = 0$. For an elastic interface, the boundary conditions are continuity in both the normal and the tangential displacement u_z and u_x, and continuity in the normal and shear stress.

A local coordinate system is used for each layer, i.e. $z = 0$ at the top of each layer, and $z = d_n$ at the bottom, where d_n ($n = 2, 3, ..., N-1$) is the thickness of layer n. Each layer is represented by a top and bottom matrix, given by [8]

$$[D_t] = \begin{bmatrix} \eta & \eta g_\alpha & C_\beta & -C_\beta g_\beta \\ C_\alpha & -C_\alpha g_\alpha & -\eta & -\eta g_\beta \\ i\rho B & i\rho B g_\alpha & -2i\rho\eta\beta^2 C_\beta & 2i\rho\eta\beta^2 C_\beta g_\beta \\ 2i\rho\eta\beta^2 C_\alpha & -2i\rho\eta\beta^2 C_\alpha g_\alpha & i\rho B & i\rho B g_\beta \end{bmatrix}, \tag{12}$$

$$[D_b] = \begin{bmatrix} \eta g_\alpha & \eta & C_\beta g_\beta & -C_\beta \\ C_\alpha g_\alpha & -C_\alpha & -\eta g_\beta & -\eta \\ i\rho B g_\alpha & i\rho B & -2i\rho\eta\beta^2 C_\beta g_\beta & 2i\rho\eta\beta^2 C_\beta \\ 2i\rho\eta\beta^2 C_\alpha g_\alpha & -2i\rho\eta\beta^2 C_\alpha & i\rho B g_\beta & i\rho B \end{bmatrix}, \tag{13}$$

respectively. In the present work, a square bracket pair [ ] is used to indicate a matrix, and a curly bracket pair { } represents a vector. A time harmonic dependency of $e^{-i\omega t}$ is assumed, and omitted for brevity [8]. For ease of notation, the following identities are introduced [8]:

$$C_\alpha = \sqrt{\left(\frac{\omega}{c_L}\right)^2 - \eta^2} = \sqrt{h^2 - \eta^2}, \qquad C_\beta = \sqrt{\left(\frac{\omega}{c_S}\right)^2 - \eta^2} = \sqrt{k^2 - \eta^2}, \tag{14}$$

$$g_\alpha = \exp\left\{ i\sqrt{\left(\frac{\omega}{c_L}\right)^2 - \eta^2}\, z \right\} = e^{iC_\alpha z}, \qquad g_\beta = \exp\left\{ i\sqrt{\left(\frac{\omega}{c_S}\right)^2 - \eta^2}\, z \right\} = e^{iC_\beta z}, \tag{15}$$

$$B = \omega^2 - 2c_S^2\eta^2. \tag{16}$$

For a system with two finite layers the resultant matrix equation is [8]

$$\begin{bmatrix} [D_{1b}] & [-D_{2t}] & & \\ & [D_{2b}] & [-D_{3t}] & \\ & & [D_{3b}] & [-D_{4t}] \end{bmatrix} \begin{Bmatrix} \{A_1^-\} \\ \{A_2\} \\ \{A_3\} \\ \{A_4^+\} \end{Bmatrix} = \begin{bmatrix} [-D_{1b}^+] & \\ & [-D_{4t}^-] \end{bmatrix} \begin{Bmatrix} \{A_1^+\} \\ \{0\} \\ \{0\} \\ \{A_4^-\} \end{Bmatrix}, \tag{17}$$

where both the left and the right hand matrix are sparse matrices, and [8, 20]

$$\{A^+\} = \begin{Bmatrix} A_{(L+)} \\ A_{(S+)} \end{Bmatrix}, \qquad \{A^-\} = \begin{Bmatrix} A_{(L-)} \\ A_{(S-)} \end{Bmatrix}, \qquad [D^+] = \begin{bmatrix} D_{11} & D_{13} \\ D_{21} & D_{23} \\ D_{31} & D_{33} \\ D_{41} & D_{43} \end{bmatrix}, \qquad [D^-] = \begin{bmatrix} D_{12} & D_{14} \\ D_{22} & D_{24} \\ D_{32} & D_{34} \\ D_{42} & D_{44} \end{bmatrix}. \tag{18}$$

By assembling the different matrices in Eq. (17), a total of $4(N-1)$ equations are found, where N is the number of layers (including halfspaces). The number of finite layers in the structure can be increased by adding additional matrices and vectors to Eq. (17) [8]. This method is also valid for a single layer in water, i.e. $N = 3$.

The pressure transmission and reflection coefficients for the layered medium are calculated by solving Eq. (17) with respect to the left hand amplitude vector, i.e. multiplying from the left with the inverse of the left hand matrix, as

$$\begin{Bmatrix} \{A_1^-\} \\ \{A_2\} \\ \{A_3\} \\ \{A_4^+\} \end{Bmatrix} = \begin{bmatrix} [D_{1b}] & [-D_{2t}] & & \\ & [D_{2b}] & [-D_{3t}] & \\ & & [D_{3b}] & [-D_{4t}] \end{bmatrix}^{-1} \begin{bmatrix} [-D_{1b}^+] & \\ & [-D_{4t}^-] \end{bmatrix} \begin{Bmatrix} \{A_1^+\} \\ \{0\} \\ \{0\} \\ \{0\} \end{Bmatrix}, \tag{19}$$

with $\{A_1^+\} = \{1, 0\}$ for fluid, and $\{A_4^-\} = \{0, 0\}$, i.e. unit amplitude of the incident longitudinal wave, and no waves propagating in the lower halfspace towards the sandwich. It is also assumed that the fluids in the upper and lower halfspaces, respectively, are equal. As in Section 2.1, the transmission and reflection coefficients are calculated from the ratio of the reflected and transmitted pressure to the incident pressure, respectively. From Eq. (19), the reflection and transmission coefficients are given as

$$R_{11}^{LL} = \frac{A_1^-}{A_1^+} = A_1^-, \tag{20}$$

$$T_{14}^{LL} = \frac{A_4^+}{A_1^+} = A_4^+. \tag{21}$$

3 Experimental setup

Two different measurement techniques are used in the present work: A) pulse-echo; and B) through-transmission. In A) a short, broad-band pulse is transmitted by the transducer, reflected from the plate, and received by the transmitting transducer. In B), a long sinusoidal burst with a single frequency is used to excite the plate, and the waveform through the plate is recorded by a needle hydrophone. The experimental setup used with the two different techniques are designated measurement setup A and B, respectively, and are discussed in detail in the following.

A list of the equipment used in the present work is given in Table 1. Figure 3 shows an illustration of the measurement setup, where the transmitter, a plate, and the receiver are placed in the tank and immersed in water.

Table 1: List of the equipment used in the present work to perform the acoustical and mechanical measurement on the different materials.

Equipment type	Manufacturer	Model
Transducer	Panametrics	V302 (1 MHz, 1 inch diameter)
Transducer	Panametrics	V307 (5 MHz, 1 inch diameter)
Power amplifier	Apex	PA09
Signal generator	HP	33120A
Pulser/receiver	Panametrics	5052UA
Needle hydrophone with preamp	Panametrics	1 mm probe
Hydrophone electronics	Panametrics	DC coupler w/ power supply
Filter	Krohn-Hite	3940
Linear motorized stage (x)	CMR	
Linear motorized stage (y)	Ealing Electro-Optics	53-8116/5
Rotational motorized stage (θ_T)	Ealing Electro-Optics	37-0379
Motor controller	Ealing Electro-Optics	DPS Controller, 37-1559
DAQ	NI	DAQPad 6015
Oscilloscope	LeCroy	WaveSurfer 424
Computer	Dell	Precision M4400
Power supply	Oltronix	B 703D
Software	CMR	TOF
Digital caliper	Mitutoyo	CD-15B
Digital weight	Sartorius	BL 310

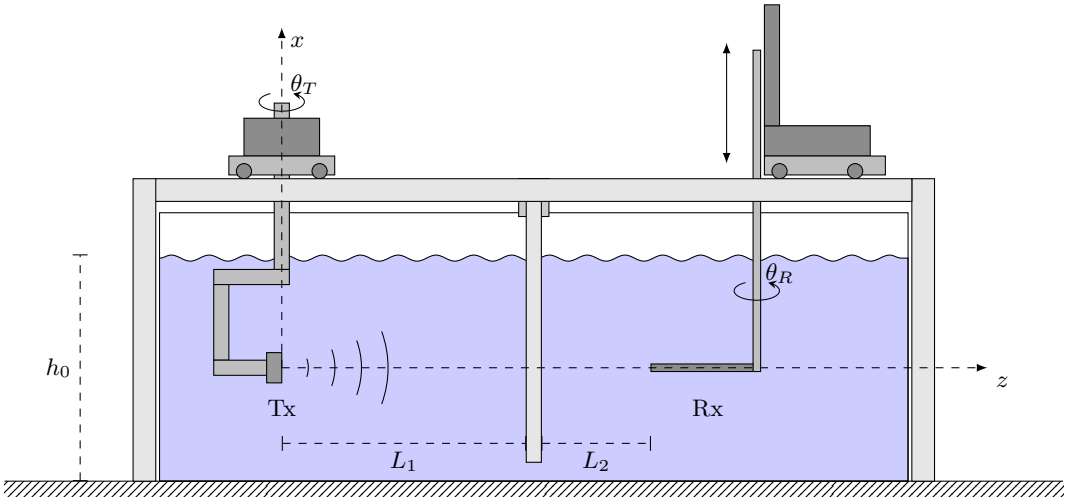

Figure 3: Illustration of the measurement setup. The transmitter is placed with the center of the front face at $x = y = z = 0$, with a distance L_1 to the front of the plate. Similarly, the receiver is placed coaxially with the transmitter, at a separation distance of L_2 between the front of the receiver and to the rear of the plate.

The experimental setup consists of three major components: A water tank; an aluminium frame; and the instrumentation. Internally, the tank is 57 cm wide, 147 cm long, and 60 cm tall. The height of the water is $h_0 = 50$ cm, which corresponds to a volume of approximately 420 L. The influence of the reflections of the acoustic waves in the tank during measurmeents is reduced by filling the tank as high as possible, and using a sufficiently low repetition rate for the transmitted waveforms.

An aluminium frame is placed on the outside of the tank to support the transmitter, the plate, the receiver, and the motorized stages. The transmitter and the receiver are mounted to separate carriages, which allows the separation distance to be varied. The transmitter is placed in a transducer mount so that the center of the front face of the transducer is aligned with the axis of rotation for the motorized stage. Similarly, the receiver is mounted to the motorized linear vertical stage,

The transmitter is aligned normal to the steel plate by visual evaluation, and by locating the maximum amplitude of the reflected pulse, without reflections in the signal. Similarly, the receiver is aligned coaxially to the transmitter. The height and tilt of the transmitter and receiver are aligned with the aid of a self-levelling cross-line laser. In the y direction, the coaxial alignment is performed by scanning the hydrophone across a line to locate the position with maximum amplitude. This is in turn also evaluated visually. The plates are mounted to the frame with two bolts and adjusted vertically using the vertical laser line.

The distance from the front face of the transmitter to the center of the plate, L_1, is approximately 20 cm, and the distance from the center of the plate to the front face of the needle hydrophone is $L_2 = 10$ cm. This corresponds to a one-way propagation time of approximately 135 µs and 67 µs, respectively.

Two different experimental setups with respect to the instrumentation are used in the present work. These are designated measurement setup A and B, respectively, and are discussed in the following.

3.1 Measurement setup A

Figure 4 shows a block diagram of measurement setup A, which is used for the pulse-echo measurements in the present work.

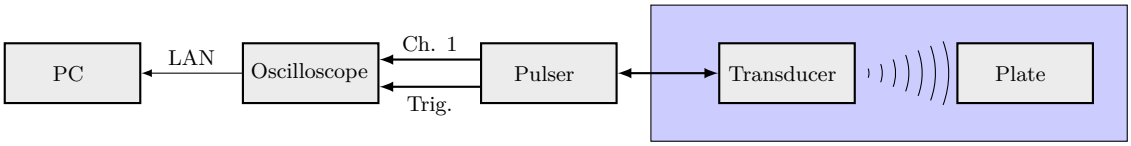

Figure 4: Block diagram of experimental measurement setup A, used for acoustical pulse-echo measurements in the water tank. The blue region indicates the components which are immersed in water.

The pulser is connected to the immersion transducer, and the output and trigger of the pulser are connected to the oscilloscope. RG-58 coaxial cables (50 Ω) are used to connect the instruments. The pulser operates in pulse-echo mode with a repetition rate of 100 Hz, the energy setting is 3, the dampening is 500 Ω, and a 28 dB attenuation of the received signal is used. The received waveforms are averaged over 128 bursts, and the results are stored manually to a local file on the oscilloscope, and transferred via LAN to the computer for processing in MATLAB 2010a.

3.2 Measurement setup B

The through-transmission measurements in the present work are peformed with the experimental setup developed and used in [21–23], along with the needle hydrophone used in [24]. Figure 5 shows a block diagram of measurement setup B.

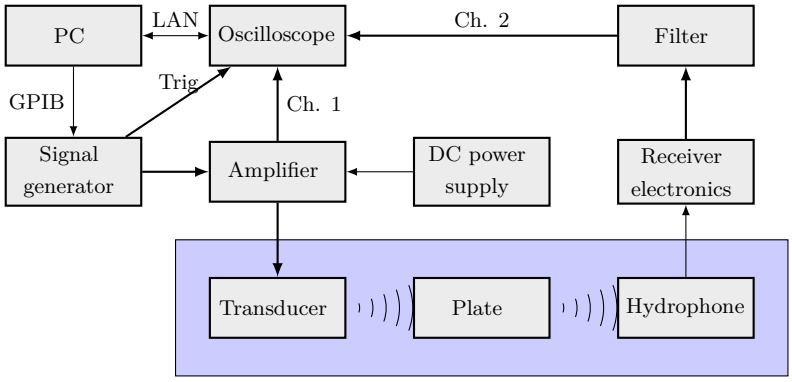

Figure 5: Block diagram of experimental measurement setup B, used for acoustical through-transmission measurements in the water tank. The blue region indicates the components which are immersed in water.

The immersion transducer is connected to the output of the Apex PA09 amplifier, which has a voltage gain of 20 dB re 1 V·V^{-1} and is driven by a ±30 V DC supply voltage. A T-coupling is connected at the output of the amplifier in order to connect the oscilloscope to channel 1, to record the voltage at the input of the transmitting transducer. The input of the amplifier is connected to the output of the signal generator.

On the receiver side, the hydrophone is connected to the combined DC-coupler and power supply, and the output is in turn connected to the input of the active filter. The latter is set up in bandpass mode, with upper and lower cutoff frequencies at 200 kHz and 2 MHz, respectively. The attenuation outside the passband is 24 dB per octave. In addition, a 20 dB re 1 V·V^{-1} voltage gain is used at the input of each of the two channels, for a total gain of 40 dB re 1 V·V^{-1} by the filter. Finally, the output of the filter is connected to channel 2 on the oscilloscope. The receiving electronics shown in Figure 5 is for the present case the combined DC-coupler and power supply for the needle hydrophone.

Instrument control and data acquisition is performed with the TOF software developed at CMR [21], which records and stores the input waveform to the transmitter, and the output waveform from the filter. The results are then processed with MATLAB 2010a, and the peak to peak input and output voltages, respectively, are calculated from the steady state region of the waveforms [23]. A frequency resolution of 2 kHz has been used from 400 kHz to 1500 kHz.

The needle hydrophone used in the present work has a length of 10 cm from the tip to the body, which is seen to reduce the reflections from the body [24], compared to the 4 cm needle used in e.g. [21, 23].

3.3 Transducer excitation signals

Figure 6 shows an example of the two types of excitation signals used in the present work: A short, broadband pulse; and a long sinusoidal burst with a single frequency.

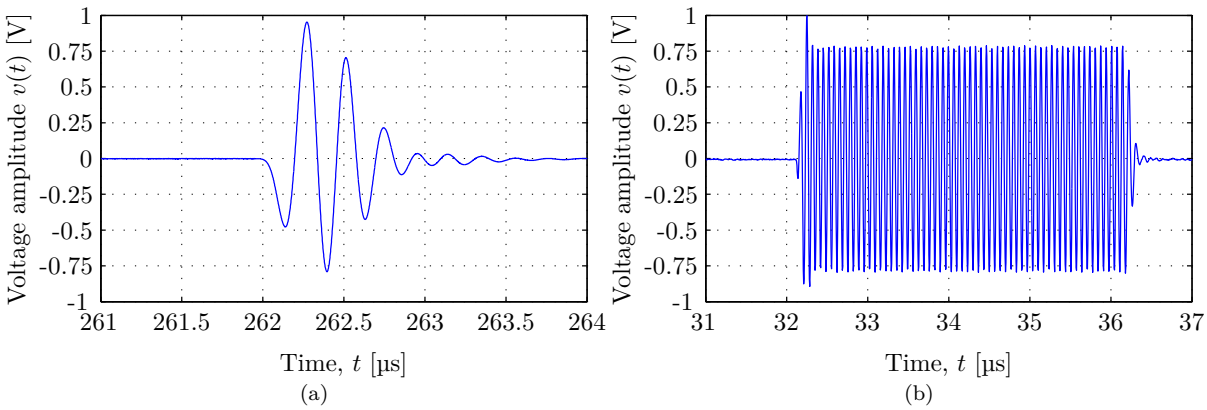

Figure 6: Example of the excitation signals used in the present work: A short broadband pulse generated by the 5 MHz transducer and the pulser (a), and a 60 cycle sinusoidal burst generated by the 1 MHz transducer and the signal generator.

The broad-band pulse in (a) is generated by applying a single period of a square wave, with a high voltage. For the 5 MHz transducer the duration the pulse is approximately 1 µs. For the sinusoidal burst shown in (b) the duration is proportional to the signal frequency, i.e. $T_p = N_p/f$, where N_p is the number of cycles. In the present work $N_p = 80$, while a 60 cycle burst is shown in (b). The output voltage of the signal generator is set to 2 V peak amplitude by the software, which is the input to the power amplifier. The waveform is in turn amplified by 20 dB re $1\,\mathrm{V{\cdot}V^{-1}}$, to a peak voltage of approximately 20 V, which is the input voltage across the terminals of the transmitting transducer. This excitation voltage is chosen to obtain the best signal to noise ratio, while reducing the non-linear effects in the transducer, and avoiding saturation of the amplifier.

3.4 Plates and sandwich construction

Two different plates are used in the present work: A 6.05 mm stainless steel plate; and a 10 mm thick Plexiglas plate, cf. Figure 7 (a). The present stainless steel plate has been investigated in several works, such as [21–25]. The steel plate has a slight curvature, as seen in Figure 7 (b). Compared to a straight edge the difference is approximately 3 mm close to the center of the plate. It is assumed that the plate is straight for the region where the main lobe of the acoustic beam impacts the plate.

Figure 7 shows a picture of the sandwich construction used in the acoustical measurements.

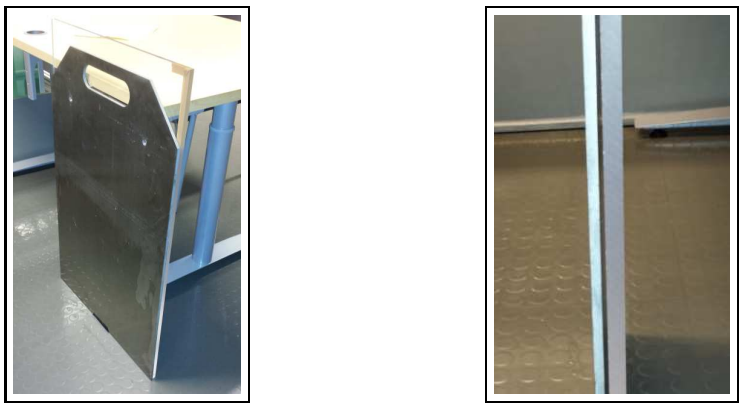

(a) (b)

Figure 7: Picture of the experimental sandwich construction (a) with the 6.05 mm stainless steel plate (front), and the 10 mm Plexiglas plate (rear), and a picture of the gap between the two plates with no clamping (b).

The sandwich is assembled by first immersing the two plates in the water tank with some spacing, and leave them immersed for a few hours to allow the amount of air bubbles to be reduced. Then, the sandwich is assembled under water by clamping the two plates together along the edge. However, by clamping the two plates together the boundary conditions of continuous displacement and traction are not fulfilled, cf. Section 2.2. Figure 8 shows an illustration of the different vibrational characteristics of the two-layer sandwich.

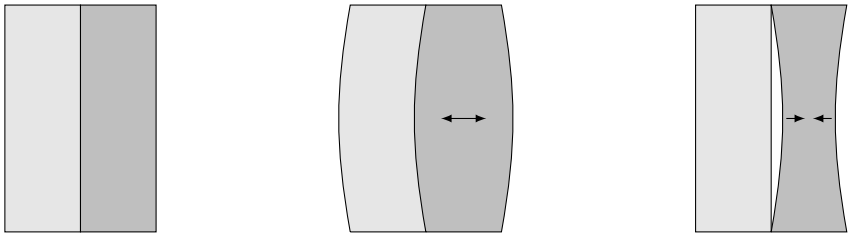

(a) (b) (c)

Figure 8: Illustration of the exaggerated displacement of a two-layered medium in vacuum. Zero movement (a), extension of the right hand plate in the thickness direction (b), and contraction of the right hand plate in the thickness direction (c).

The motionless case is shown in (a) as a reference, where the two plates are in contact along the boundary. In (b), a displacement is imposed on the right hand plate so that it extends in the thickness direction, forcing a displacement of the left hand plate. In (c) the right hand plate contracts in the thickness direction, and the movement does not affect the left hand plate. If perfect bonding was present in (c) the left hand plate be displaced in such a manner that there is continuity along the boundary.

Proper bonding cannot be obtained simply by clamping the two plates together; a thin film of glue, epoxy or similar is required. This however, affects the behaviour of the vibration. Such effects are discussed in e.g. [24] for a piezoceramic electric transducer construction. In the present case the two plates cannot be glued together since a non-invasive bonding method is required.

3.5 Transmission and reflection coefficients

As discussed in Section 2.1, the transmission coefficient is defined as the pressure incident at the plate, divided by the pressure at the rear of the plate. With plane waves and lossless materials, the incident pressure can be calculated in an arbitrary position in front of the plate, and similarly for the transmitted pressure. This is not the case for the acoustical measurements, where attenuation in the water must be taken into account, along with the diffraction effects due to the finite size of the transmitter.

In the present work, the acoustical measurements have been performed with the transmitter and receiver stationary to ensure that their alignment is equal for each case. Thus, the transmission coefficient is not calculated explicitly, it is approximated by a normalized pressure given as

$$T(f) \approx \frac{V_p(f)}{V_w(f)}, \tag{22}$$

where V_p and V_w are the voltage spectra with and without the plate present, respectively. It is assumed that this approximation is sufficiently accurate for the present analysis.

4 Results

4.1 Material characterization

A summary of the material parameters used in the simulations of the different materials is given in Table 2.

Table 2: List of material data for the different materials used in the present work. The sound velocities for the Plexiglas are calculated using acoustical spectroscopy with a 1 MHz transducer pair.

Material	c_L [m·s^{-1}]	c_S [m·s^{-1}]	ρ_0 [kg·m^{-3}]	α [dB·MHz^{-1}·cm]	d [mm]
Steel [22]	5780	3130	8000	0	6.05
Plexiglas	2730	1300	1190	1.13 [26]	10.0 ± 0.2
Water	1483	0.001	1000	0	-

A small but non-zero value for the shear sound velocity in water is used to avoid numerical problems in the simulations. The measured values for the two sound velocities in the Plexiglas are in correspondence with other values reported in the literature, e.g. [27], and the attenuation coefficient is used to compensate the measurements.

4.2 Transducer response in water

Figure 9 shows the magnitude of the frequency spectrum of the received signal in water, $V_w(f)$, for the 1 MHz transducer. The maximum in the magnitude is -19.6 dB re 1 V·V^{-1} at 1166 kHz. A flat region is observed from 770 kHz to 800 kHz, at -25 dB re 1 V·V^{-1}. Oscillations are seen in the magnitude from 400 kHz to 800 kHz.

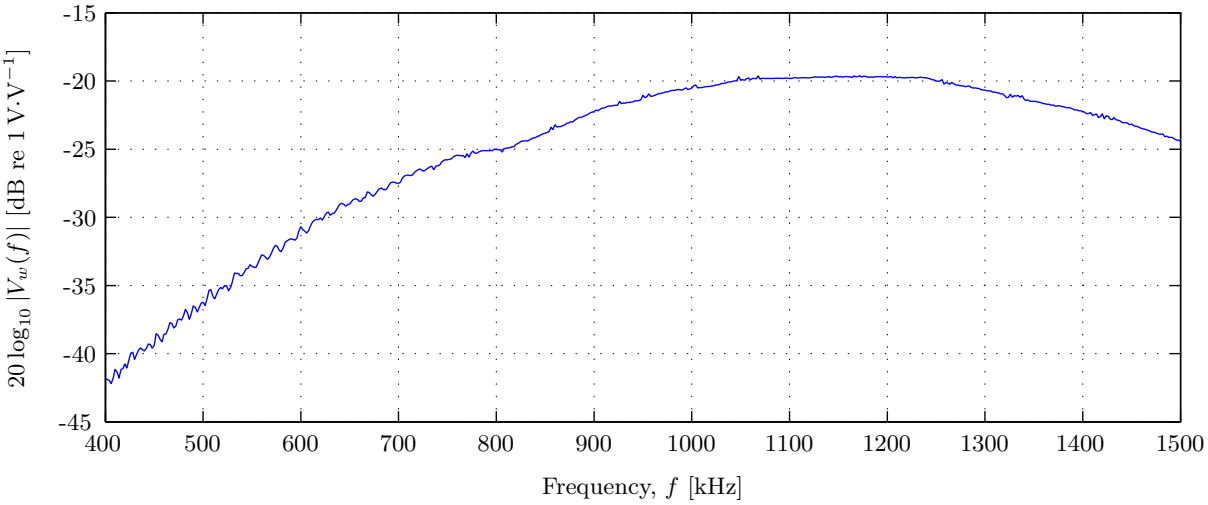

Figure 9: Magnitude of the frequency spectrum for the received signal in water, $V_w(f)$, for the 1 MHz immersion transducer. The measurement is performed with experimental setup B without the plate present.

4.3 Stainless steel plate immersed in water

Figure 10 shows a comparison between the normalized pressure from the measurement, and the transmission coefficient T_{LL} for the 6.05 mm stainless steel plate immersed in water, calculated with GMM at normal and 1° incidence, respectively.

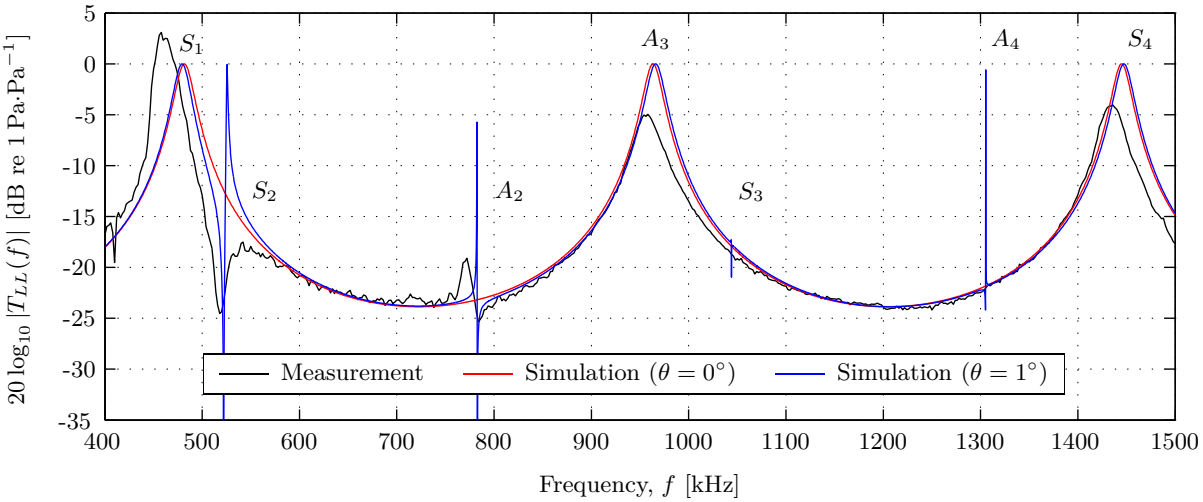

Figure 10: Magnitude of the pressure transmission coefficient for the 6.05 mm stainless steel plate immersed in water, calculated with GMM at normal incidence (red) and 1° incidence (blue), and compared to acoustical measurements with single frequency of the normalized pressure (black). The S and A markers indicates the Rayleigh-Lamb modes for the stainless steel plate in vacuum.

In the simulation at normal incidence (red curve) the peaks in the transmission coefficients are located at the longitudinal resonance frequencies, cf. Eq. (11), which in the present frequency range are 482 kHz, 964 kHz, and 1446 kHz, with a magnitude of 0 dB re 1 Pa/Pa. These frequencies corresponds to the S_1, A_3, and S_4 modes, respectively, cf. Eqs. (9) and (10). Away from these modes the magnitude is decreasing towards a minimum value of -23.8 dB re 1 Pa/Pa.

When the incidence angle in the simulation is increased to 1° (blue curve), shear modes are excited in the plate, and a frequency shift is observed at the thickness resonance frequencies. At the A_1 mode the peak is shifted down by 2.4 kHz compared to the normal incidence case, while at the two higher modes an increase of 2.7 kHz and 2.0 kHz is observed, with no reduction in magnitude. The shear modes in the simulation are located near 523.5 kHz, 782 kHz, 1044 kHz, and 1306 kHz, for the S_2, A_2, S_3, and A_4 modes, respectively. The S_2 mode is seen to have a fairly large width in frequency, while the higher order modes are more narrow, especially S_3 and A_4.

Compared to the simulation at normal incidence the peaks in the measurements which corresponds to the A_3 and S_4 modes have a -5.2 dB and -4.0 dB difference in magnitude, and a shift of approximately 8 kHz and 10 kHz, respectively. The S_2 and A_2 modes are also visible in the measurements. For the S_2 mode a minimum is seen at 518 kHz with a magnitude of -24.5 dB re 1 Pa/Pa. The A_2 mode has a larger extent in frequency compared to the simulation with a maximum value of -19.1 dB re 1 Pa/Pa at 772 kHz. Compared to the simulation results, the S_1 mode has a peak with a magnitude of 3.1 dB re 1 Pa/Pa at 458 kHz, i.e. a 24 kHz frequency shift and an increase in magnitude compared to the plane wave model. This behaviour, along with the reduction in magnitude for the A_3 and S_4 modes, has been discussed by e.g [21–24, 28].

Away from the different modes, the behaviour and magnitude of the measurement is in fair correspondence with the simulations. Some ripples are observed in the measurement below the A_3 mode with peak to peak variation of approximately 1 dB re 1 Pa·Pa^{-1}. Measurements on the present steel plate in previous work, e.g. [22], has shown better correspondence between the measurements and simulations with respect to the frequency of the A_3 mode. The difference in the present work is assumed to be caused by improper alignment of the transmitter, plate, and receiver.

4.4 Plexiglas plate immersed in water

Figure 11 shows the magnitude of the pressure transmission coefficient T_{LL} for the 10 mm Plexiglas plate immersed in water, measured with the needle hydrophone and compared to simulations at normal incidence calculated with GMM.

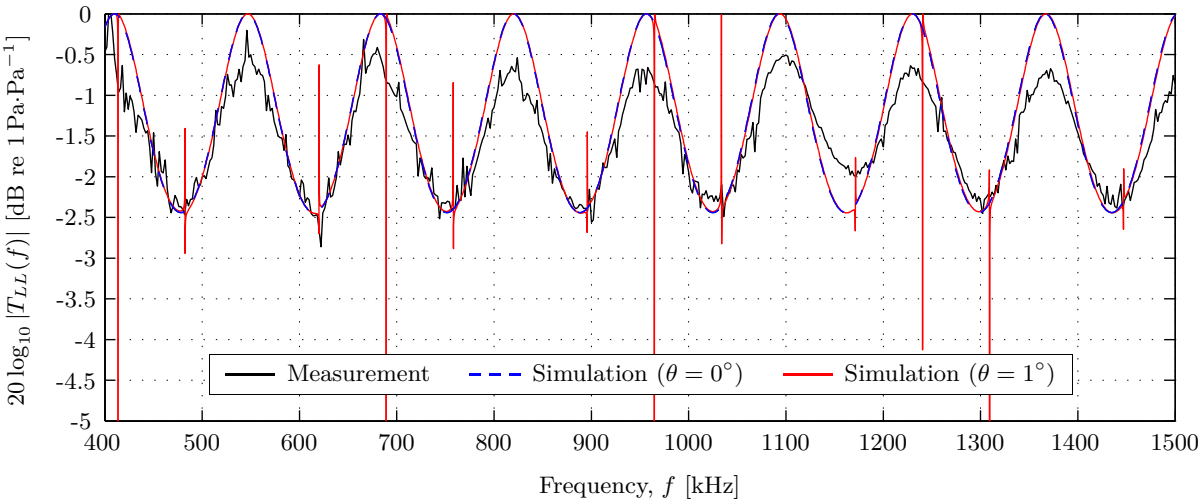

Figure 11: Magnitude of the pressure transmission coefficient T_{LL} for the 10 mm Plexiglas plate immersed in water, calculated with GMM at normal incidence (blue dashed) and 1° incidence (red), and compared to acoustical measurements with single frequency of the normalized pressure (black).

Compared to the steel plate, the resonance frequencies are more closely spaced for the Plexiglas, due to the relatively low sound velocity and large plate thickness, cf. Eq. (11). The first peak in the magnitude of the simulation results, within this frequency range, has a frequency of 409.5 kHz with a magnitude of 0 dB re 1 Pa·Pa^{-1}, and the higher order modes are equidistantly spaced by 136.5 kHz, cf. Eq. (11) and Table 2. Similarly, the first minimum in the simulation results is located at 477.75 kHz with a magnitude of -2.45 dB re 1 Pa·Pa^{-1}. The higher order minima are also equidistantly spaced by 136.5 kHz, with the same value for the magnitude since the material is lossless in the simulations.

The magnitude of the maxima in the measurement results is seen to decrease with increasing frequency, from -0.2 dB re 1 Pa·Pa^{-1} at 546 kHz to -0.67 dB re 1 Pa·Pa^{-1} at 1372 kHz. In the present case, a frequency dependent term has been added to the magnitude of the measurements to account for the attenuation in the Plexiglas, which is significant within this frequency range. This term is 1.13 dB·cm^{-1}·MHz^{-1} re 1 Pa·Pa^{-1} [26].

In the minima of the measurement results, fair correspondence is observed compared to the magnitude of the simulation results, i.e a magnitude of approximately -2.5 dB re 1 Pa·Pa^{-1}. One distinct exception is the minimum near 1170 kHz, where the magnitude is -2 dB re 1 Pa·Pa^{-1}, i.e. a difference of 0.4 dB compared to the simulation.

For 1° incidence, shear modes are excited near the minima in the magnitude of the simulation results, and at every second peak. The modes are fairly narrow in frequency, typically 5 kHz. A significant amount of ripples is observed in the measurement results. Consequently it is difficult to identify any shear modes in the measurements, such as e.g at 622 kHz and 900 kHz. As for the measurements on the steel plate, these ripples are assumed to be caused by improper alignment of the transmitter, plate, and receiver.

4.5 Sandwich construction immersed in water

Figure 12 shows the magnitude of the pressure transmission coefficient T_{LL} for the 6.05 mm stainless steel plate (black), the 10 mm Plexiglas plate (red), and the sandwich construction (blue), immersed in water, calculated at normal incidence with GMM. In the following, the terms S and A are used in the discussion of the sandwich construction, which refer to the symmetric and antisymmetric modes for the steel plate immersed in fluid, as

discussed in Section 4.3.

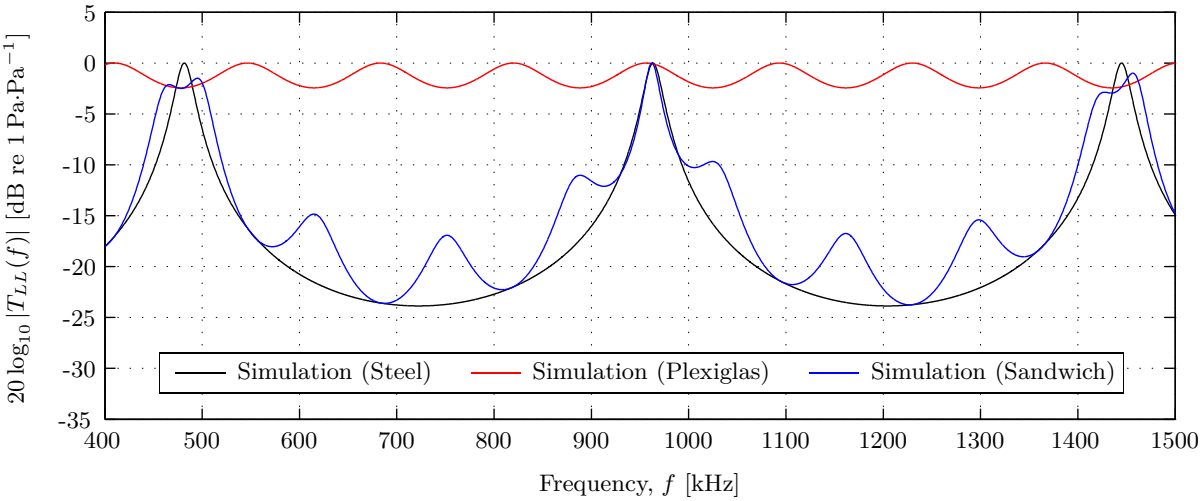

Figure 12: Magnitude of the pressure transmission coefficient T_{LL} for the 6.05 mm stainless steel plate (black), the 10 mm Plexiglas plate (red), and the sandwich construction (blue), immersed in water, calculated at normal incidence with GMM.

The magnitude for the sandwich construction is seen to be a combination of the two components, i.e. there are three significant peaks which corresponds to the steel plate resonance frequencies, and oscillations (with relative higher frequency) which corresponds to the Plexiglas plate. For the latter case, a 180° phase shift is found between the max/min for the sandwich, compared to the single Plexiglas plate immersed in water. The minimum magnitude for the sandwich construction appears to be limited to that of the steel plate, except in the regions near the steel plate thickness resonance frequencies. Near the S_1 and S_4 modes for the steel plate, a reduction in magnitude is found and it is observed that the peaks for the steel plate coincides with minima for the Plexiglas plate. Near the A_3 mode for the steel plate, a peak is also observed in the magnitude for the Plexiglas plate. Consequently, a similar reduction in the magnitude for the sandwich is not observed. At 615 kHz an increase of 6.8 dB is observed compared to the steel plate. This increase is also found for the peaks at 752 kHz, 888 kHz, 1025 kHz, 1161 kHz, and 1298 kHz.

The overall increase in magnitude of the transmission coefficient for the sandwich, compared to the steel plate, is assumed to be a result of the increased coupling between the steel and the water, due to the Plexiglas plate: The characteristic impedance of the Plexiglas is higher than for water, and thus it acts as a matching layer.

At normal incidence, the difference between the local maxima away from the thickness resonance frequencies of the steel plate could be used to estimate either the thickness of the Plexiglas or the longitudinal sound velocity. However, calculation of one of these parameters requires that the other parameter is known.

Figure 13 shows the magnitude of the measured pressure transmission coefficient for the sandwich construction immersed in water, compared to the acoustical measurement on the steel plate presented in Figure 10 (black), and a simulation of the transmission coefficient for the sandwich calculated with GMM at normal incidence.

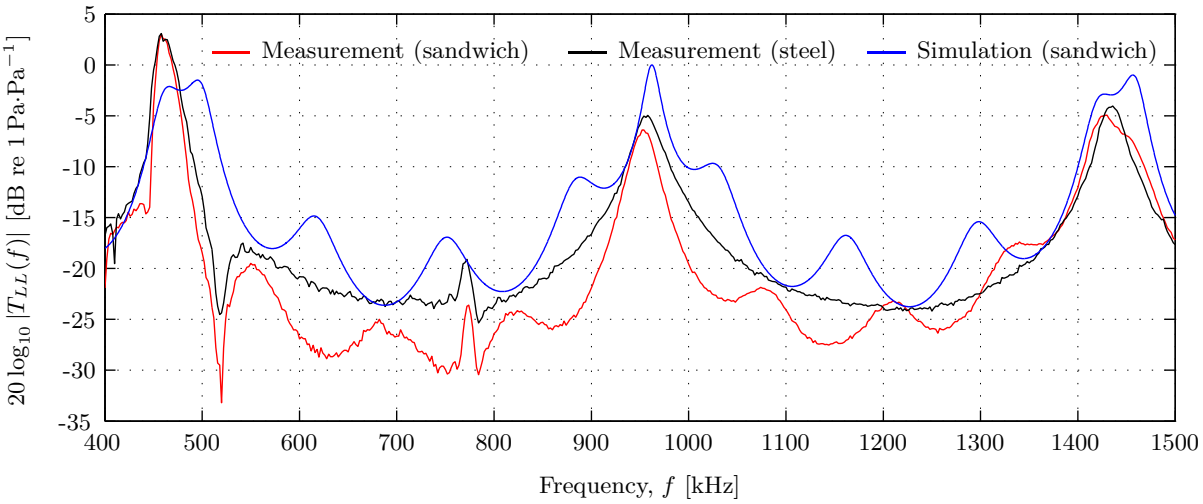

Figure 13: Magnitude of the measured pressure transmission coefficient T_{LL} for the sandwich construction immersed in water (red), compared to the magnitude of the measured transmission coefficient for the steel plate (black), compared to a simulation calculated with GMM of the sandwich at normal incidence (blue).

The simulation results shown in Figure 12 indicates that the overall transmission is increased for the steel plate when the Plexiglas layer is attached. This is not so for the measurements on the steel plate shown in Figure 13, where an overall reduction in magnitude is observed when the Plexiglas is included. The magnitude at the S_1 mode is equal for both the measurement on the sandwich and on the steel plate separately. The minimum near the S_2 region is more distinct for the sandwich measurement, with a difference of 8.8 dB at 520 kHz. The A_2 mode of the steel plate is also present near 770 kHz, with a reduction in magnitude compare to the steel plate.

At the A_3 mode for the steel plate near 960 kHz the peak is more narrow for the sandwich than for the steel plate, and the magnitude is reduced by 1.4 dB for the sandwich. Near the S_4 mode the peak is more wide for the sandwich than for the steel plate, with a reduction of 1.7 dB at 1438 kHz.

Oscillations in the magnitude are also observed in the measurement of the sandwich, similar to those in the simulation. However, local maxima of these oscillations appear to coincide with local minima in the simulation, and *vice versa*. This can be seen near e.g. 682 kHz, 822 kHz, 1076 kHz, 1210 kHz, etc. The frequency spacing between these maxima is approximately 130 to 140 kHz, which corresponds well with the theoretical spacing between the resonance frequencies in the single Plexiglas plate, cf. Figure 11 and Eq. (11).

4.6 Sandwich construction immersed in water - Influence of debonding on transmission

The difference observed in Figure 13 between the measurements and simulations on the sandwich construction is assumed to be caused by the lack of proper bonding between the two plates, cf. the discussion given with Figure 13. While it is for the present case not possible to adjust the measurement setup to that of the simulations, the simulation model can be adjusted to include debonding between the plates. To investigate this a thin layer of water with thickness h_w is introduced between the two plates in the simulation model, i.e. adding an additional layer to the sandwich model. This fluid layer also eliminates the shear coupling between the two plates, i.e. $\tau_{xz} = 0$, so that the only shear waves propagating in the Plexiglas plate are generated from mode conversion of the incident longitudinal waves. The thickness of the water layer is varied in steps from 0 to 1 mm, which is an estimate of the plausible range for the experimental setup when the sandwich is clamped together. The aim is to investigate if a similar behaviour as in the measurements is introduced in the simulation results, i.e. a reduction in magnitude away from the resonance frequencies for the steel plate, and if the maxima and minima of the oscillations are interchanged and dependent on the fluid thickness.

Figure 14 shows the magnitude of the pressure transmission coefficient for the sandwich construction with

a fluid layer between the plates, calculated with GMM at normal incidence as a function of frequency and fluid thickness. The case for $h_w \equiv 0$ corresponds to the simulation result shown in Figure 13 with bonding between the plates.

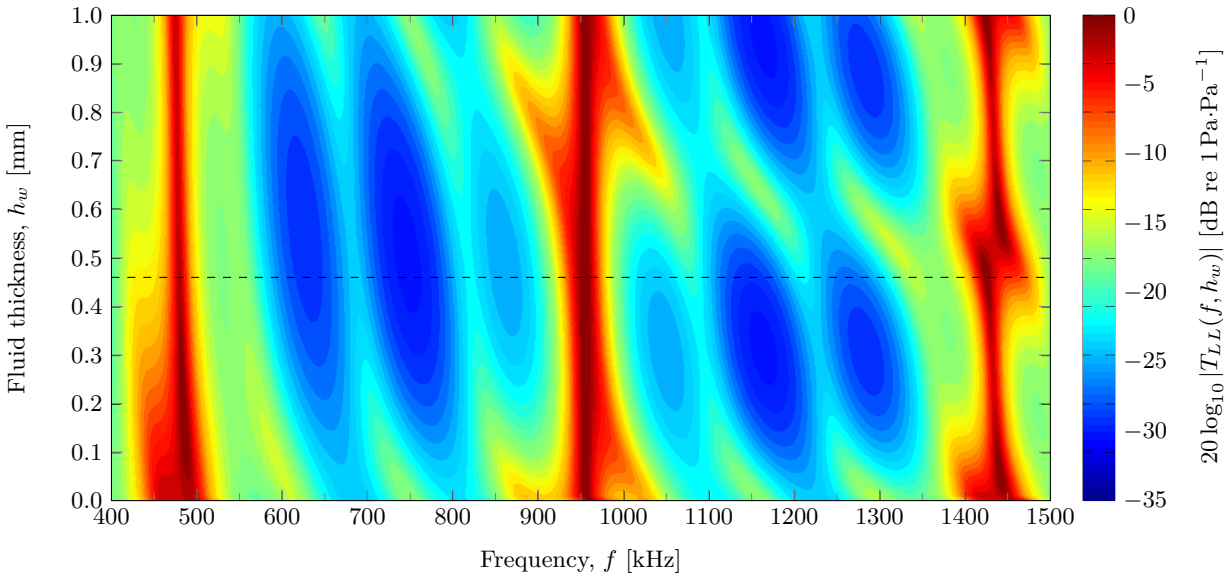

Figure 14: Magnitude of the pressure transmission coefficient T_{LL} for the sandwich construction immersed in water, calculated with GMM at normal incidence as a function of frequency and fluid thickness h_w between the two plates. The case with bonding between the plates is shown for $h_w = 0$. The dashed horizontal line indicates $h_w = 0.46$.

For the case with bonding, i.e. $h_w = 0$, the maxima in the magnitude of the transmission coefficient are seen near 482 kHz, 964 kHz, and 1446 kHz, as shown in Figure 12. Similarly, the local maxima away from these frequencies are seen near 615 kHz, 752 kHz, 1161 kHz, and 1298 kHz.

As the fluid thickness is increased, the peaks near the longitudinal resonance frequencies for the steel plate become more narrow. For the local maxima, a downward shift in the frequency is observed, along with a reduction in magnitude compared to the bonded case.

From $h_w = 0.5\,\text{mm}$ and beyond, a maximum is observed near 1200 kHz which also decreases in frequency and magnitude as the thickness is increased. Similar behaviour is also observed for the maximum near 1300 kHz. This is very similar to the behaviour seen when the thickness is increased from 0.

A qualitatively similar behaviour as that observed in the measurements is seen near $h_w = 0.5\,\text{mm}$: Compared to the bonded case, the width of the first and second maxima is decreased, the local maxima are minima, and the magnitude away from the peaks is reduced. Based on these constraints, analysis of Figure 14 indicates that $h_w = 0.46$ is the best match for the present case.

Figure 15 shows the magnitude of the pressure transmission coefficient T_{LL} for the sandwich construction immersed in water, measured with the needle hydrophone and compared to simulations at normal incidence calculated with GMM as a function of frequency, and simulation at normal incidence with a water layer of thickness $h_w = 0.46\,\text{mm}$ between the plates.

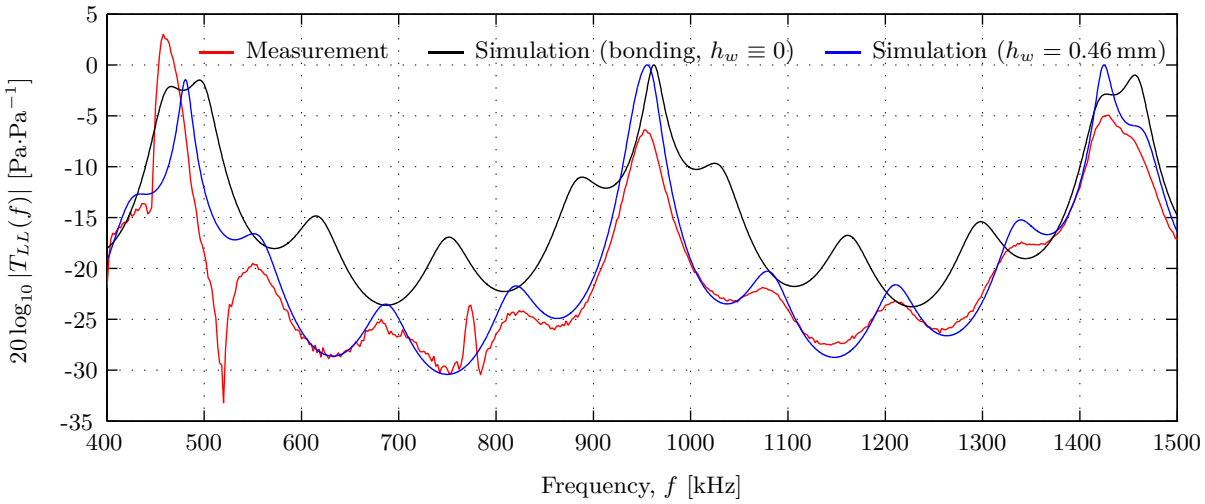

Figure 15: Magnitude of the pressure transmission coefficient for the stainless steel/Plexiglas sandwich construction immersed in water, calculated with GMM at normal incidence (black), compared to acoustical measurements with single frequency (red), and compared to a simulation with GMM for a debonded sandwich with a water layer which is $h_w = 0.46$ mm thick (blue).

With the 0.46 mm thick fluid layer introduced in the simulations, a better overall correspondence is observed between the magnitude of the measurements and simulations, compared to the simulation with bonding ($h_w = 0$). A better agreement is observed for both the magnitude and frequency of the local maxima and minima due to the Plexiglas, cf. Figure 11. The width of the peak near the S_2 steel plate mode, has decreased compared to the case with bonding.

Below A_1 the peaks which originates from the Plexiglas are seen to be "in phase" with the peaks for the Plexiglas plate in water. This is in correspondence with the discussion for the sandwich, where the two cases are in opposite phase due to the difference in matching. With debonding, the Plexiglas plate has fluid loading at either side, where the characteristic impedance is lower than for the Plexiglas. For the sandwich with bonding, one side on the Plexiglas has a steel loading, where the impedance is higher than for the Plexiglas. Consequently there is a 180° phase difference between these two cases [29].

A perfect agreement between the measurements and simulations are not expected based on the difference observed for the steel plate and Plexiglas immersed in water. However, the results indicates that the debonding is the cause of the difference between the measurements and simulations of the sandwich.

4.7 Sandwich construction immersed in water - Influence of debonding on reflection

Figure 16 shows the magnitude of the pressure reflection coefficient for the sandwich construction, compared to the results for the steel plate and Plexiglas plate separately immersed in water.

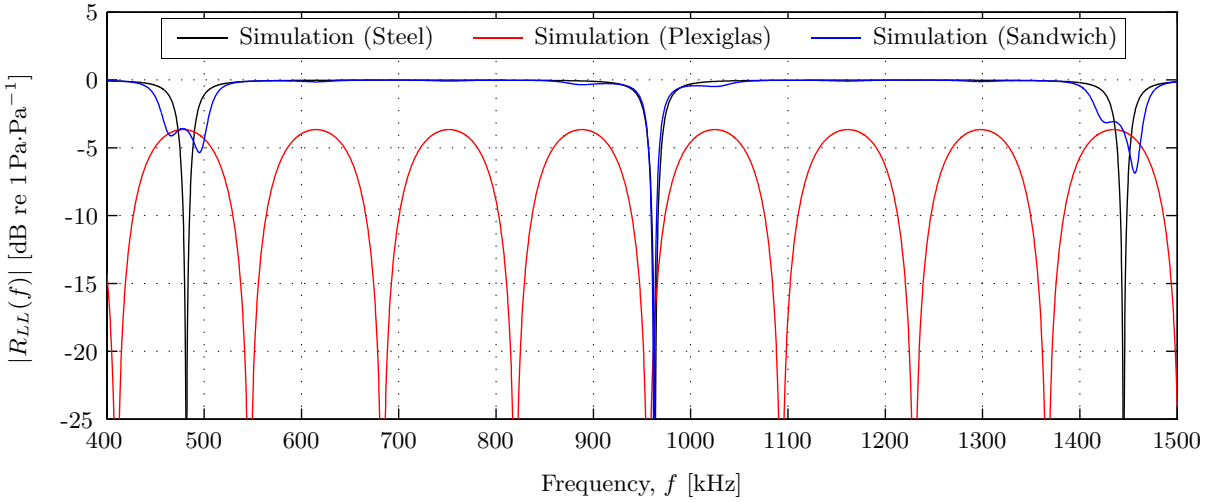

Figure 16: Magnitude of the pressure reflection coefficient R_{LL} for the 6.05 mm stainless steel plate (black), the 10 mm Plexiglas plate (red), and the sandwich construction (blue), immersed in water, calculated at normal incidence with GMM.

For the steel plate (black curve) an overall high magnitude, approximately -0.02 dB re 1 Pa·Pa^{-1}, is observed, except for the regions close to the thickness resonance frequencies of the plate. This is expected, since a high transmission through the plate corresponds to low reflection, and *vice versa*.

The maxima in the magnitude for the Plexiglas plate (red curve) at minima in the transmission coefficient, and the maximum magnitude is -3.67 dB re 1 Pa·Pa^{-1}. Compared to the steel plate, the overall magnitude for the Plexiglas is lower due to the high transmission through the Plexiglas plate, which is related to the low characteristic impedance.

In the magnitude for the sandwich construction (blue curve), the oscillations due to the Plexiglas plate are visible, but far less distinct compared to in the magnitude of the transmission coefficient, cf. Figure 12. Near the resonance in the steel plate at 964 kHz, the magnitude for the sandwich is low due to the coincidence between a minimum for the steel plate and the Plexiglas, respectively. However, the reflection coefficient is relatively high near the steel plate resonance frequencies at 482 kHz and 1446 kHz, respectively. At 478 kHz the magnitude is -3.59 dB re 1 Pa·Pa^{-1} for the sandwich, which is an increase of 0.08 dB compared to the Plexiglas case. A relatively high reflection coefficient at these frequencies is due to the contribution from the Plexiglas plate.

The effects of debonding between the steel plate and the Plexiglas plate can also be observed in the time domain waveforms for a short pulse. When good bonding is present, the Plexiglas acts as a matching layer to water, and the energy of the wave is allowed to escape more quickly compared to the steel plate with water coupling.

Figure 17 shows an example of the reflected time domain waveform from the single steel plate, and from the sandwich construction, respectively. A 5 MHz transducer with a short pulse is used (cf. Figure 6 (b)), operating in pulse-echo mode. In the present case, a time correction is introduced to align the first pulse of the two waveforms, and the amplitudes are normalized to their respective maximum values.

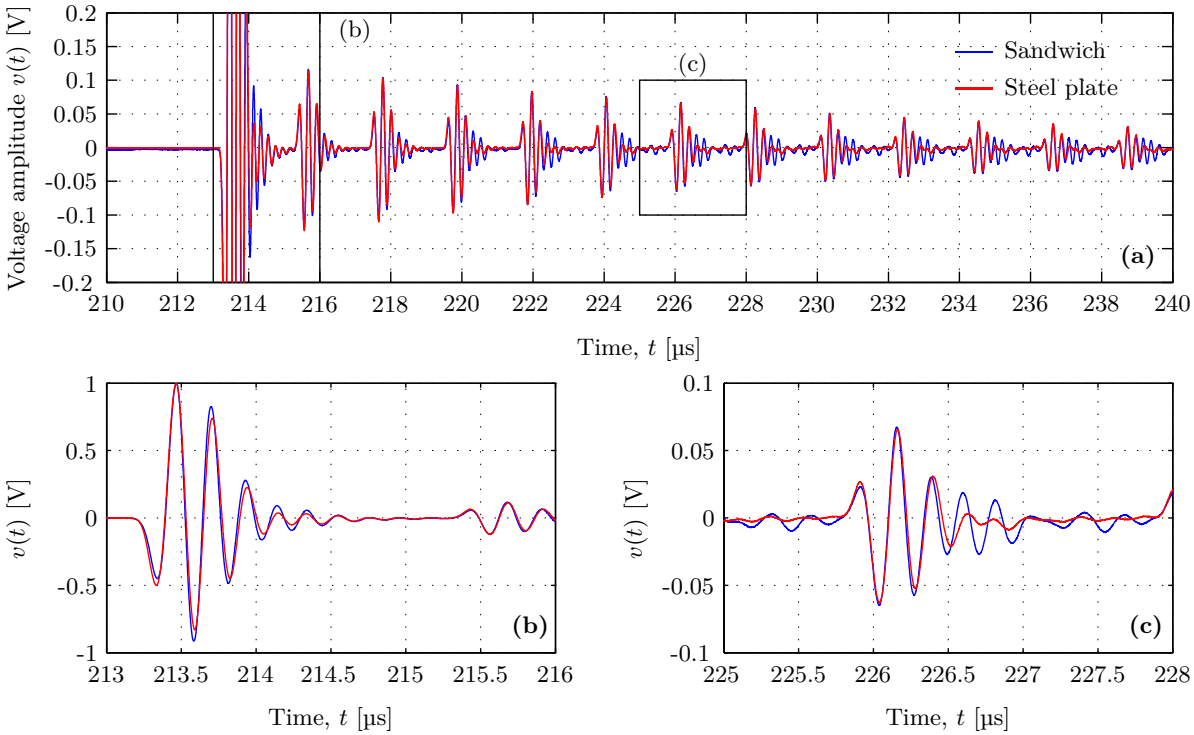

Figure 17: Time domain waveform of the reflected signals from the sandwich construction (blue) and the single steel plate (red), normalized in amplitude and aligned in time, measured with the 5 MHz immersion transducer in pulse-echo mode at normal incidence (a). A closeup of the first pulse is shown in (b), and a closeup of a trailing pulse near $t = 226\,\mu s$ is shown in (c).

The relative decay of the amplitude of the trailing pulses for the measurements on the sandwich, is seen to be fairly equal to that for the steel plate immersed separately in water. This indicates that there is a lack of bonding between the two plates in the sandwich, since the Plexiglas should increase the coupling between the steel plate and the water, thereby increasing the amount of energy which escapes the steel plate.

The internal reflected pulses in the sandwich after approximately 219 µs are seen to have a longer length than their steel plate counterparts. This corresponds to the two-way propagation time of 7.3 µs for a pulse in the Plexiglas plate, i.e. the first reflection from the Plexiglas/water interface. This pulse is in turn transmitted back into the steel plate and propagates towards the receiver, along with a corresponding series of internal reflections in the steel plate.

5 Conclusions

In the present work, the transmission coefficient for a two-layered elastic medium immersed in water which consists of a 6.05 mm stainless steel plate and a 10 mm Plexiglas plate, has been investigated at normal incidence from 400 kHz to 1500 kHz with acoustical measurements, and compared to simulations using the global matrix method.

The characteristic behaviour of the transmission coefficient for the stainless steel plate and the Plexiglas plate immersed in water, are identified both experimentally and with simulations in the results for the sandwich construction. These results can be used to identify the different materials, based on some prior knowledge.

A fairly significant difference between the simulations of the transmission coefficient for the sandwich construction with bonded plates, and the acoustical measurements is observed. This is shown with simulations to be caused by an improper bonding for the experimental sandwich, by including a thin layer of fluid in the simulations and performing a systematic analysis. Results are also presented for pulse-echo measurements on the sandwich to illustrate the debonding between the plates.

Acknowledgements

The present work has been financed by PETROMAKS 2/The Norwegian Research Council, project number 225965/E30. Gaute Lied at CMR is acknowledged for assistance with the software for the experimental setup. The Acoustics group at the University of Bergen is acknowledged for the loan of the needle hydrophone.

References

[1] American Petroleum Institute, "Recommended Practice for Testing Well Cements, Second Edition (API RP 10B-2)", (2013).

[2] M. W. Ewing, W. S. Jardetzky, and F. Press, *Elastic waves in layered media*, 1st edition, McGraw-Hill Book Company, Inc., New York, (1957).

[3] J. D. Achenbach, *Wave propagation in elastic solids*, 1st edition, American Elsevier Publishing Company, Inc., New York, (1973).

[4] L. M. Brekhovskikh, *Waves in layered media*, 2nd edition, Academic Press, Inc., New York, (1980).

[5] A. Ben-Menahem and S. J. Singh, *Seismic waves and sources*, 2nd edition, Dover Publications, Inc., New York, (2000).

[6] J. Pujol, *Elastic wave propagation and generation in seismology*, 1st edition, Cambridge University Press, Cambridge, UK, (2003).

[7] J. M. Hovem, "Acoustic waves in finely layered media", Geophysics **60**(4), 1217–1221 (1995).

[8] M. J. S. Lowe, "Matrix techniques for modeling ultrasonic waves in multilayered media", IEEE Trans. Ultrason. Ferroelectr. Freq. Control **42**(4), 525–542 (1995).

[9] W. T. Thomson, "Transmission of elastic waves through a stratified solid medium", J. Appl. Phys. **21**, 89–93 (1950).

[10] N. A. Haskell, "Dispersion of surface waves on multilayered media", Bull. Seism. Soc. Am. **43**, 17–34 (1953).

[11] L. Knopoff, "A matrix method for elastic wave problems", Bull. Seism. Soc. Am. **54**, 431–438 (1964).

[12] M. J. Randall, "Fast programs for layered half-space problems", Bull. Seism. Soc. Am. **57**, 1299–1316 (1967).

[13] D. L. Folds and C. D. Loggins, "Transmission and reflection of ultrasonic waves in layered media", J. Acoust. Soc. Am. **62**(5), 1102–1109 (1977).

[14] COMSOL Inc., "COMSOL Multiphysics ® Modeling Software", `http://www.comsol.com/`.

[15] E. Bossy, "SimSonic - FDTD simualtion of ultrasound propagation", `http://www.simsonic.fr/`, Accessed: 06/05-2014.

[16] B. E. Treeby and B. T. Cox, "*k*-Wave: MATLAB toolbox for the simulation and reconstruction of photoacoustic wave-fields", J. Biomed. Opt. **15**(2) (2010).

[17] P. Lunde, "Lecture notes in the course PHYS374 - Theoretical acoustics", Department of Physics and Technology, University of Bergen (2010).

[18] J. L. Rose, *Ultrasonic waves in solid media*, Cambridge University Press, Cambridge, UK, (1999).

[19] J. W. Dunkin, "Computation of modal solutions in layered elastic media at high frequencies", Bull. Seism. Soc. Am. **55**, 335–358 (1965).

[20] B. Pavlakovic and M. J. S. Lowe, "DISPERSE - A system for generating dispersion curves, User's manual (Version 2.0.16b) ", Imperial College of Science, Technology and Medicine, London, UK, 2003.

[21] K. D. Lohne, M. Vestrheim, and P. Lunde, "Ultrasonic signal transmission in steel plates", in *Proceedings of the 31st Scandinavian Symposium on Physical Acoustics, Geilo, Norway, 27-30 January 2008*, edited by U. Kristiansen, Norwegian Physical Society, (2008).

[22] K. D. Lohne, P. Lunde, and M. Vestrheim, "Measurements and 3D simulations of ultrasonic directive beam transmission through a water-immersed steel plate", in *Proceedings of the 34th Scandinavian Symposium on Physical Acoustics, Geilo, Norway, 30 January - 2 February 2011*, edited by R. Korneliussen, Norwegian Physical Society, (2011).

[23] K. D. Lohne, "Transmission of 3-D ultrasonic directive beams through a water immersed steel plate. Experimental and simulation results", PhD thesis (in preparation), Department of Physics and Technology, University of Bergen, Bergen, Norway.

[24] M. Aanes, "Interaction of piezoelectric transducer excited ultrasonic pulsed beam with fluid-embedded viscoelastic plate", PhD thesis, Department of Physics and Technology, University of Bergen, Bergen, Norway (2014).

[25] M. Aanes, K. D. Lohne, P. Lunde, and M. Vestrheim, "Ultrasonic beam transmission through a water-immersed plate at oblique incidence using a piezoelectric source transducer. Finite element - angular spectrum modeling and measurements", in *Proceedings of the IEEE International Ultrasonics Symposium, Dresden, Germany, 7 - 10 October 2012*, 1972–1977, IEEE, (2012).

[26] S. Umchid, "Frequency dependent ultrasonic attenuation coefficient measurement", in *Proceedings of the 3rd International Symposium on Biomdical Engineering, 10-11 November Bangkok, Thailand*, , (2008).

[27] A. Zerwer, M. A. Polak, and J. C. Santamarina, "Wave propagation in thin Plexiglas plates: implications for Rayleigh waves", NDT & E International **33**, 33 – 41 (2000).

[28] M. Aanes, K. D. Lohne, E. Storheim, P. Lunde, and M. Vestrheim, "Beam transmission of water-embedded steel plate at normal incidence. Diffraction effects in the S_1 to A_3 region", in *Proceedings of the 38th Scandinavian Symposium on Physical Acoustics, Geilo, Norway, 1 - 4 February 2015*, edited by R. Korneliussen, Norwegian Physical Society, (2015).

[29] L. E. Kinsler, A. R. Frey, A. B. Coppens, and J. V. Sanders, *Fundamentals of Acoustics*, 4th edition, John Wiley & Sons, New York, (2000).